Understanding how arc attachment behaviour influences the prediction of composite specimen thermal loading during an artificial lightning strike test

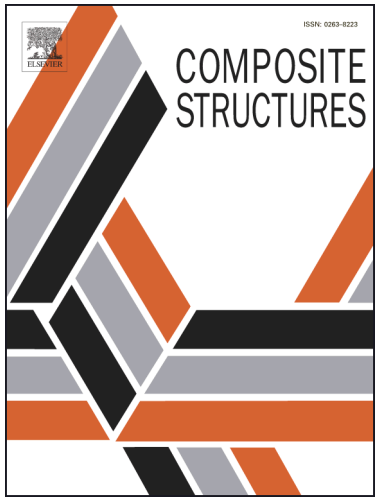

Understanding how arc attachment behaviour influences the prediction of composite specimen thermal loading during an artificial lightning strike test

P. Foster, G. Abdelal, A. Murphy

PII: S0263-8223(18)30416-1
DOI: https://doi.org/10.1016/j.compstruct.2018.03.039
Reference: COST 9486

To appear in: *Composite Structures*

Received Date: 26 January 2018
Revised Date: 1 March 2018
Accepted Date: 12 March 2018

Please cite this article as: Foster, P., Abdelal, G., Murphy, A., Understanding how arc attachment behaviour influences the prediction of composite specimen thermal loading during an artificial lightning strike test, *Composite Structures* (2018), doi: https://doi.org/10.1016/j.compstruct.2018.03.039

Understanding how arc attachment behaviour influences the prediction of composite specimen thermal loading during an artificial lightning strike test

P Foster [a], G Abdelal[a], A Murphy [a,+]

[a] *School of Mechanical and Aerospace Engineering, Queen's University Belfast, Ashby Building, Belfast. Northern Ireland, U.K. BT9 5AH*

[+] *Corresponding author: Tel.: +4428 9097 4095; E-mail: a.murphy@qub.ac.uk*

Abstract

High speed image analysis of experimental lightning strike testing on composite specimens has demonstrated complex time-dependent arc attachment behaviour. To date simulation studies of lightning strike direct effects on composite materials have overlooked or idealised the observed arc attachment behaviour. This is significant as these preceding studies have also demonstrated joule (resistive) heating is a major contributor to composite material damage and thus the application of the current load is critically important. The objective of this paper is to quantify how arc attachment behaviour influences the prediction of composite specimen thermal loading during a simulated lightning strike test. This is achieved through a simulation study modelling experimental arc attachment behaviours referenced in the literature. The simulation results are compared with measured test specimen damage. The results quantify for the first time the significance of arc attachment behaviour, demonstrating how realistic representation of arc expansion and arc movement can alter the predicted thermal loading and generate thermal damage patterns comparable to measured experimental damage.

Keywords: Lightning Strike; lightning arc attachment; thermal-electric loading; composite damage; Finite Element Modelling.

1.0 Introduction

The use of composite material in the manufacture of civil transport aircraft has increased rapidly in recent years and it is now widely used in empennage, wing and fuselage structure. This includes the extremities of the aircraft which are the typical location for initial attachment of the lightning arc [1]. Like any lightning event an aircraft lightning strike is a complex coupled phenomenon made up of electrical, magnetic, thermal and mechanical components [2]. Lightning strikes can have a detrimental effect on composite structures if they are not protected via specialised surface materials (typically metal meshes or paints) [3-6]. Compared with metals composites have poor electrical properties due primarily to the properties of the polymer constituent and the isolating nature of reinforcing fibre lamination within the polymer (with the fibres typically possessing good electrical conductivity). It is understood that the application of significant electrical and thermal energy at the lightning arc attachment point will cause a large build-up of local material temperature, via joule heating and heat transfer from the arc attachment, which can result in catastrophic material damage [7].

To date test standards representing the features of real world lightning events have been developed and are used to ensure that lightning protection systems can safely shield the underlying composite materials during the service life of an aircraft [8-11]. Variants of such test procedures have also been used to understand how the design parameters of a composite material and the parameters of the test arrangement influence the scale and form of material damage with and without protection systems [3-5, 12-25]. However, due to the experimental challenges associated with lightning strike testing (the high energy involved, the short duration of the event, the limited number of facilities and resulting cost and waiting time [26]) a body of computational research has also evolved which attempts to model the standard tests. The general objective of such modelling work is to enable the prediction of

the physical behaviours during a strike to understand how damage is caused and how protection systems can be improved [3-6].

However, to date the computational research has not accurately represented the complex time-dependent arc attachment behaviour which has been witnessed during a number of the experimental works [16, 18, 20-21]. Thus this paper investigates the potential contribution of arc attachment behaviour on computational prediction of composite specimen thermal loading and resulting damage. This is achieved through a simulation study building on established modelling approaches [26-34]. The study examines the observed arc behaviour from the literature [16, 18, 20-22] and represents the significant features of the behaviour within the established modelling framework, comparing the predicted damage with the measured test specimen damage. The following section outlines the experimental arc attachment behaviour in the literature and the approaches used thus far in the literature to model the arc attachment within simulations for the prediction of direct effects (i.e. material damage). This section is followed with details on the proposed modelling approach, followed by a series of simulation case studies and experimental comparisons, which together enable the assessment of the influence of current load modelling on composite damage prediction. The paper is concluded with a summary of the key findings and proposed future steps to improve lightning strike modelling and testing.

2.0 Background

A number of experimental studies have been carried out on a range of composites specimens under artificial lightning strikes which loosely adhere to the SAE standards [10]. The

artificial lightning strikes are generally carried out by applying a large current through an impulse generator. This supplies a large current over a short period of time to the composite plate specimen via a discharge probe held close to the centre of one face of the specimen. The opposite face or edges of the specimen are typically connected to earth to permit the current to travel through the specimen. Generally the probe is a small distance from the specimen to ensure that it strikes the specimen towards its centre.

Katunin et al. [3-4] tests a novel material system, developed to reduce material damage during a lightning strike. Wang et al. [5] experimentally examines a number of protection systems including their method of application. Hirano et al. [17] conducted a range of tests on pristine unnotched specimens. Feraboli et al. [16, 18] tested a range of current loading on specimens with and without fasteners. Kawakami et al. [20-21] carried out a comprehensive study examining a range of current loading, materials and specimen stacking sequences. Munoz et al. [25], as far as the authors are aware is the only published work to apply the maximum current load defined in the standards (Waveform-A).

Reviewing these experimental works the post-test damage is consistently identified as material ablation, fibre breakage, thermal decomposition, ply lift and matrix cracking (inter and intra ply). Moreover three damage areas are identified but inconsistently labelled. These include two surface damage areas, herein labelled the ‘severe damage area’ and the ‘moderate damage area’. The severe damage area generally penetrates several ply layers depending on the size of the artificial current load and includes resin thermal decomposition (evidenced by char residue) with signs of mechanical force present (some sharp resin morphology, fractured fibres, fibres blown outwards). The moderate damage area is a wider but shallower area confined to a small number of the plies at the surface of the specimen and contains the severe damage area. In this case there is some thermal decomposition and signs of mechanical force present (sharp and shiny resin morphology, fractured fibres which appear to have been blown

out of the resin). In addition there is typically subsurface damage present, herein labelled the 'subsurface damage', where matrix cracking takes the form of intralaminar matrix cracking and delamination which can extend below the specimen surface and beyond the visible surface damage perimeter. Figure 1 presents damage measurement analysis for two specimens tested by Hirano et al. [18] and subjected to a peak current test load of 40kA. In the figure the shapes and dimensions of the three noted damage areas (severe, moderate and sub-surface) are determine using image analysis software.

Significantly a small number of these experimental works have also captured the arc attachment behaviour during the test. In particular in reviewing experimental images during the lightning strike with high speed video recording [16, 20] and observations by other experimental authors [18, 21-22, 35-36] there are four observed characteristics:

- The arc channel expands over time, a number of authors have proposed that expansion occurs due to build-up of energy which heats and expands the air at the strike point [22, 35-36].
- Arc expansion occurs principally in the direction perpendicular to the specimen surface fibres, due to large potential gradients in that direction [20] (as less current flows in the transverse direction due to lower electrical conductivity).
- A filament of more dense current is concentrated at the centre of the channel.
- The arc filament is not stationary and the attachment point moves position during the strike.

Although these behaviours are uncertain in nature a number of authors have attempted to quantify their magnitude. Kawakami [20] captures simultaneously in photographs the arc channel expansion parallel and perpendicular to the surface fibre directions allowing directional scaling of the expansion. Chemartin et al. [22] proposes an arc radius versus time

graph which is dependent on the magnitude of the peak current applied. Kawakami [20] identifies a brighter filament of arc in the centre of the lightning throughout the event but in this case is unable to apportion any magnitude. Likewise, arc movement is referenced but not quantified [20, 35-36].

Given the noted experimental works there is still incomplete understanding of the relationships and damage mechanics which occur during a lightning strike test. Simulation can allow for a more direct analysis on how damage is formed, allowing the representation of damage initiation and propagation. So far numerical work has mostly focused on modelling resistive heating from the electrical load [29-34] but other loading mechanics have also been studied (electromagnetic and acoustic pressure [25-26], internal blast loading [33]) but with significantly less attention. The resistive heating models predict the temperature field in the specimen based on the applied electrical load (thermal-electric analysis) – modelling the conversion of electrical energy into thermal energy. The predicted temperature fields are then used to assess the level of damage, either using a simple set of temperature rules, e.g. [25, 29] or an integrated analysis decomposition model which can represent changing electric and thermal-electric properties with temperature and/or heating rate during the thermal-electric analysis, e.g. [30-31].

Four works attempt to replicate the experimental work carried out by Hirano et al. [17], and follow one another progressively in so far as they attempt to better the prediction of the experimentally measured damage. Ogasawara et al. [29], Abdelal and Murphy [30], Wang et al. [31] and Dong et al. [32] apply the current profile used experimentally by Hirano et al. [17]. In addition Liu et al. [33] also follows Hirano's [17] experimental work but uses a smaller current peak load (10kA). Ogasawara et al. [29] applies the current load to the plate through one node at the plate centre. Abdelal and Murphy [30] applies the load uniformly over a circular area with a radius of 5mm and uses a circular partition at the plate centre to

apply the load. Dong et al. [32] states the load is applied over a circular area with a radius of 2.5mm. Wang et al. [31] and Lui et al. [33] do not state how their current load was applied. One lightning author [37] is found to model non-uniformity and expansion of the arc channel however this load is applied as a thermal load to a glass fibre composite. Due to the poor electrical conductivity of glass fibres compared with carbon fibres, the physics of this event differs from lightning strikes to CFRPs. In addition each author represents the plate dimensions and layup with some differences. For example Ogasawara et al. [29] models a total specimen thickness of 4 mm versus the 4.704 mm of the experimental work and performs a post analysis correction. Abdelal and Murphy [30] use a quarter model and therefore do not represent fully the specimen stacking sequence properties. Wang et al. [31] and Lui et al. [33] only use eight plies (32 in the experiment) thus have modelled fewer thicker plies.

The major modelling developments relate to improvements in the material property representation. Ogasawara et al. [29] initially modelled non-temperature dependent material properties and predicted unrealistically high temperatures (>100,000°C). Thus all authors introduce temperature dependent properties (e.g. thermal & electrical conductivities, specific heat, density) with each author attempting to better represent how the thermal-electric material properties vary with temperature and to capture the relationship between the material decomposition and the instantaneous material properties. Given the extreme conditions being modelled for most properties the proposed material relationships have necessarily been extrapolated from experimental data generated from lower temperature and heating rate tests. Finally Abdelal and Murphy [30] and Wang et al. [31] introduce modelling strategies to represent the ablation of plies. In Abdelal's case [30] this is achieved by effectively modelling through-thickness infinite electrical conductivity for the local ply element once the model predicts local temperatures to cause ablation. In Wang's case [31] by deleting elements

and reapplying the load at the next stacking sequence layer once the model predicts local temperatures to cause material ablation.

Figure 2 presents the predicted simulation results for the five simulations [29-33]. As the authors have used a range of damage criteria the peak temperatures are plotted for consistency. Examining the temperature fields it is possible to recognise similarities between the predictions and consistent differences when compared with the experimental damage measurements, Figure 1. The temperature contours from all simulations have a similar shape: narrow and elongated in the surface ply fibre direction. A visual inspection of the simulated temperature fields and the experimental damage show that the extreme simulation temperatures are oriented along the surface ply fibre direction whereas the experimental damage areas are oriented along the 0° direction, Figure 1. Thus the greatest difference between the predicted damage in the preceding works and the measured damage has been damage width and orientation. Also considering the depth of damage, the experimental work identified damage down to the fifth ply from the struck surface. Abdelal and Murphy [30] predict damage to the 4^{th} ply, Ogasawara et al. [29] > 6^{th} ply, and Dong et al. [32] to the 9^{th} ply. In all cases the damage area below the surface extends beyond the surface damage area, something not measured experimentally.

Munoz et al. [25] created models of the acoustic pressure and electromagnetic effects, for two different test waveforms. Results indicated that electromagnetic/acoustic effects were not enough to cause significant damage alone but when combined with thermal effects could produce matrix cracking and delamination. Foster et al. [26] modelled a number of proposed pressure shockwave loads from the literature and compared the predictions with measured test specimen damage. The results indicate that although a pressure load can cause damage consistent with that measured experimentally, it has a negligible contribution to the overall scale of damage.

In summary while simulations so far have confirmed the widely held view that resistive heating is significant the details of the predictions do not compare well with experimental measurements, neither in the surface damage (area and shape) or depth of damage (including profile). Due to the application of a uniform electric current load through a single node or over a constant radius (2.5 or 5 mm) the preceding idealisation of a fixed, concentrated electrical load has potentially resulted in unrepresentative electrical energy being dissipated along a narrow band of surface fibres. Moreover the concentration of electrical load may also have resulted in more rapid through thickness heating leading to accelerated through thickness electrical conductivity and unrepresentative energy dissipation through the specimen thickness. The literature review finds that the electrical load is not applied using experimentally observed lightning channel behaviour. Numerical models apply the electrical load as a constant and uniform electrical load whereas the lightning channel is observed to expand, elongate in the transverse direction, have a non-uniform distribution and move during the strike.

3.0 Methodology

This section briefly introduces thermal electric modelling, the experimental test setup and specimen to be simulated and the methodologies proposed to improve the representation of arc attachment behaviour.

The flow of electric current in a material is governed by electric potential difference, in our case the potential between the arc attachment and the grounded face of the test specimen. Joule heating arises when such current flow is converted into thermal energy and

such heating can then change material properties and thereby change the current flow. In addition the converted thermal energy may then be transferred through the material via thermal conduction or given enough energy can lead to a change of state of the material (again changing material electric properties). Thus due to the coupled thermal-electric behaviour between electrical potential and temperature fields it is necessary to solve both fields simultaneously. This is achieved herein using temperature dependent electrical properties, the Finite Element (FE) method and the coupled thermal-electric equations in a two-step simulation procedure (in the commercial software ABAQUS [38]). For the relevant governing equations, described in the context of lightning strike modelling, readers are initially referred to the works of Wang and Zhupanska [37, 41].

From the literature review it can be seen that the experimental work carried out by Hirano et al. [17] has received the greatest attention, for the most part as it provides the greatest information in terms of the description of the experimental setup and resulting damage. Hence numerical simulations herein attempt to simulate Hirano's experiment. Hirano's experimental specimen is 150x100 mm and contains 32 plies each with a thickness of 0.147mm. The material is IM600/133 and the ply layup is $[45/0/-45/90]_{4s}$. In the experimental test the probe is held approximately 3 millimetres above the composite plate and hence the arc is assumed to initially attach at the specimen centre. The composite specimen is set on a copper plate which acts as an earth. A zero potential boundary condition is applied to the bottom surface of the specimen to replicate the function of the experimental copper plate. Discharge was also witnessed from the edges of the specimen and thus zero potential boundary conditions are also applied at the specimen edges.

The analysis is carried out in two steps: a fully coupled thermal-electric step is used during which the electrical load is applied and resistive heating occurs. This step is carried out using thermal-electric elements (DC3D8E) and solved using a transient solution

procedure due to the speed of the event. A second step, using a heat transfer solution procedure and the same element type and mesh then models the heat dissipation through the specimen after the strike allowing sufficient time for heating to occur in lower plies. The review of numerical simulations has demonstrated that a temperature dependent material model is important and thus temperature dependent thermal/electric properties proposed by Abdelal and Murphy [30] are used with some adjustments based on Hirano's experimental work [17]. Table 1 presents the material properties used in all simulations. Abdelal uses a different through thickness electrical conductivity to that measured by Hirano [17]. Herein we use Hirano's measured through thickness electrical conductivity of 1.79×10^{-6} 1/Ωmm. In addition herein the temperature range associated with resin decomposition is modelled as 500°C and 800°C (modelled between 300°C and 500°C by Abdelal), based on thermogravimetric analysis (TGA) by Ogasawara et al. [29]. Kawakami suggests that explosive moisture vaporisation causes moderate damage and Li [39] finds there is a greater damage area and depth with increased moisture in the composite. Again using Ogasawara's TGA data moisture loss is assumed to occur at 300°C (not modelled but a monitored boundary at which damage with very rapid heating is possible). Through-thickness electrical conductivity remains the same until fibre ablation occurs at which point the current load is then transferred to the element below by giving the ablated element an infinite electrical conductivity. The temperature range associated with fibre decomposition remains the same as modelled by Abdelal, 3,316°C to 3,334°C. Finally, energy released during resin decomposition is assumed to be 4.8×10^{6} J, between 500°C and 800°C and the energy released during fibre ablation is assumed to be 43×10^{6} J, between 3,316°C and 3,334°C [40].

The key behaviour during the analysis is located at the centre of the specimen and therefore a simulation mesh was developed which was refined at the centre and coarsened toward the specimen edges. A mesh convergence study was undertaken which examined the

predicted temperature contour at the specimen surface (total area above 300 and 500 °C) and the predicted temperature contour through the specimen depth (total area above 500 °C). Convergence was considered to have occurred with an in-plane mesh seed of 1.5 mm and 2 elements through the thickness of each of the top 8 plies. Figure 3 illustrates the final specimen mesh used in all analysis along with an overview of the analysis boundary conditions.

The electric current load with respect to time is applied to an area at the centre of the specimen using a series of surface current loads. The shape of each surface current load is defined using a field equation which enable circular and elliptical load patterns. Using multiple surface current loads and by varying their amplitude with time it is possible to create an expanding arc radius to represent the experimental current profiles. Figure 4 illustrates the method used to introduce the current loading. Each new load, with a larger radius, is introduced every 2.5×10^{-6} seconds and the previous load with a smaller radius is effectively cancelled. The loads are introduced and cancelled using an amplitude function, by raising the amplitude from zero and then reducing the amplitude back to zero. A total of 12 different loads are introduced during the loading phase of the simulation. Equations 1 and 2 present the field equations used to define a circular and elliptical loading area respectively. In both equations $\lfloor z \rfloor$ is the largest integer less than or equal to z, and $\lceil z \rceil$ is the smallest integer greater than or equal to z. In Equations 1 and 2, $x = y = z = 0$ describes the centre point on the top surface of the specimen. In Equation 1 (circular arc) r is the radius of the arc over which the load is applied. In Equation 2 (elliptical arc) a and b are the principal radii of the arc over which the load is applied. This approach also enables representation of a central filament of arc at the centre of an expanding arc. For example a percentage of the electric load can be assigned to a fixed radius circular load and a remaining percentage of the electric load can be assigned to a transversely expanding current load.

$$Field = \left\lceil \left\lfloor \frac{r}{\sqrt{x^2+y^2}} \right\rfloor \Big/ \left(\left\lfloor \frac{r}{\sqrt{x^2+y^2}} \right\rfloor + 1 \right) \right\rceil \quad \text{Equation 1}$$

$$Field = \left\lceil \left\lfloor \frac{1}{\sqrt{\frac{x^2}{a^2}+\frac{y^2}{b^2}}} \right\rfloor \Big/ \left(\left\lfloor \frac{1}{\sqrt{\frac{x^2}{a^2}+\frac{y^2}{b^2}}} \right\rfloor + 1 \right) \right\rceil \quad \text{Equation 2}$$

4.0 Results

In order to understand the relative influence of arc expansion and arc movement a series of simulations are performed (first a stationary expansion arc, then a moving non expanding arc and finally an expanding and moving arc). In each case temperature contours on the surface and through the specimen depth are compared. The temperature boundaries of 300°C, 500°C, 800°C and 3,316°C are generally considered in each case: moisture vaporisation occurs at 300°C, 500°C and 800°C are the heating rate adjusted temperatures at which resin decomposition is modelled to initiate and be completed, 3,316°C is the temperature at which fibre ablation is modelled to initiate. Before considering the individual simulation case studies a general description of the electric and thermal behaviour generally witnessed in all simulation results is presented.

4.1 General behaviour

Initially when the current is applied to the specimen the conductivity of the material in the fibre direction is significantly greater than the transverse and through thickness directions, Table 1. Although there are unequal distances to be travelled by the current to reach earth boundary conditions (at the edge of the specimen or the earthed plate below) the resistance of the path in the fibre direction is significantly less than that of the transverse and through-thickness directions. As a result initially most current flows in the fibre direction, some current flows in the transverse direction and a small amount flows in the through-thickness direction.

The significant current flow in the top ply produces resistive heating and between 500˚C and 800˚C the transverse and through-thickness electrical conductivity increases due to resin decomposition. At 800˚C the through thickness conductivity is approximately 18 times smaller than the conductivity in the fibre direction. As a result proportionally more electric current begins to flow through the thickness of the ply than flows in the ply fibre direction. Similar to the first ply and due to the lag between current flow and temperature rise the current in the second ply will initially flow in the fibre direction. A pattern thus emerges were, initially, the majority of the current flow is in the ply fibre direction before resistive heating elevates the temperature above 500˚C when a greater proportion of current then begins to flow through the thickness of the ply. As the current flow progresses through the specimen thickness a stacking sequence dependent temperature distribution is thus created.

4.2 Arc expansion results

An initial simulation replicates the arc load used by Abdelal and Murphy [30]; with two further simulations then considering a static expanding arc:

- CASE 1 – The current load is applied within a circular load radius of 5mm throughout the analysis based on predictions by Chemartin et al. [22].
- CASE 2 – The arc radius expands throughout the analysis as a circular load with a rate of expansion corresponding to Chemartin's arc radius versus time model [22].
- CASE 3 – The load expands transverse to the surface fibre direction throughout the analysis and is applied as an elliptical shaped uniform current load. The rate of expansion corresponds to Chemartin's arc radius versus time model and the area of the current load ellipse is equivalent, with time, to the circular arc defined by Chemartin and used in CASE 2. The ratio of arc channel expansion (surface fibre direction versus perpendicular to surface fibre direction) is taken from Kawakami's photographed ratio of arc expansion [20].

In each case the same total current load (i.e. action interval) and the same rate of current load is applied. Figure 5 presents the temperature contours for the simulation results. Table 2 presents the predicted area in each simulation above 500°C which represents the first point of damage initiation (resin decomposition). The 300ºC temperature contour is also described which represents vaporisation of moisture (and may cause moderate damage). Temperatures above 800ºC are negligible and not presented. Using a constant load radius of 5mm, the shape of the temperature contours are similar to previous simulations, i.e. narrow, all temperatures are oriented along the surface fibre direction and there is little change of the width of the 300ºC contour from the plate centre to the plate edge - it is severely elongated. With the introduction of circular expansion of the load, the 500ºC contour is not oriented along the fibre direction and the width of the 300ºC contour has increased, however it remains severely elongated. With the introduction of transverse expansion the 500ºC contour is cross-shaped and oriented along the 45º and -45º directions. The 300°C contour only elongates at the plate centre and the extreme width of the contour. Like Case 1 and 2 the shape is also dissimilar to

experimental moderate damage. In each case the area over 500°C increases but all are notably smaller than the areas measured experimentally, which are associated with moderate and severe damage.

4.3 Non-uniform arc results

Two simulations consider a non-uniform arc:

- CASE 4 – 50% of the current load is applied through a central fixed arc filament (CASE 1) and 50% of the current load is applied through a transversely expanding arc component (CASE 3).
- CASE 5 – Again 50% of the current load is applied through a central fixed arc filament of 5mm and 50% applied through an expanding elliptical arc component. In this case the expanding electrical load is assumed non-uniform with the current reducing linearly from the centre of the specimen to zero at the edge of the expanding arc.

Figure 6 presents the temperature contours and Table 3 presents the predicted area in each simulation above 500°C and 300ºC. Examining Figure 6 and Table 3 the surface temperatures above 500°C are restricted to a central area, with a relatively symmetric pattern, not significantly beyond the area over which the arc load was applied. The predicted areas with a temperature above 500°C remain notably smaller than the areas measured experimentally which are associated with moderate and severe damage.

Although the shape of the 500°C contour is rectangular and thus similar to the shape of experimental severe damage there are clear portions extending along the -45° axis, transverse to the surface ply fibre direction. Considering the depth of temperature penetration both simulations predict temperatures over 500°C and 800°C beyond the fifth ply. However

cross-sectional microscopy of the experimental specimens shows that the severe damage area is very small by the fourth and fifth plies. This suggests that the representation of the electrical load is too concentrated. Like Cases 3, the 300°C contour only elongates at the plate centre and the extreme width of the contour with little elongation between. The shape is dissimilar to experimental moderate damage and may also be because the load is too concentrated. Authors have observed that the arc channel moves during tests. This behaviour has not been simulated by previous authors.

4.4 Arc movement results

Three simulations initially consider arc movement:

- CASE 6 – a fixed radius arc channel with a uniform current load is moved in a single direction. The radius of the moving filament is 5 mm, the same as modelled in the previous studies and based on arc modelling by Chemartin at al. [22]. As no experimental data is available which defines an arc movement pattern, magnitude or rate, in this first simulation a transverse movement is initially assumed. The load is applied with the same method used previously to model arc expansion - via analytical fields located at each position which have their individual amplitudes varied to model the movement, Figure 7. A movement of three arc diameters is initially modelled with a load sequence starting in the centre position and then looping to one side, back to centre, then to the other side, and back to centre, repeat. The arc position dwells on each location for 2.5×10^{-6} seconds ($1/12^{th}$ of the overall period of load application) before moving. Given no experimental data is available for the movement length and dwell time each of these initial assumptions are varied in the subsequent simulations.

- CASE 7 – the same as CASE 6 but with the total width of movement increased to four arc diameters (same sequence order and dwell time). This will enable a first assessment of the influence of arc movement length.
- CASE 8 – the same as CASE 7 but with the dwell time in each location reduced to $1.0x10^{-6}$ seconds (same sequence order). This will enable a first assessment of the influence of arc dwell time.

As before in each case the same total current load (i.e. action interval) and the same rate of current load is applied. Figure 8 presents the temperature contours for the simulation results. Table 4 presents the predicted area in each simulation above 500 °C.

Examining Figure 8, for all cases the predicted surface area over 500°C is larger compared with previous simulations. In CASE 6 a clear portion of the area above 500°C is now oriented along the 0° axis (the direction of modelled arc movement) and a portion of the area above 500°C which is oriented along the +45° axis (the surface fibre direction). In CASE 7 the arc movement is increase by a third resulting in a greater portion of the area above 500°C oriented in the direction of the arc movement, with a smaller portion extending as one strand away from the strike centre, oriented along the surface fibre direction. The predicted area above 500°C has also increased – by 11%, with the length of the 500°C contour approximately 41 mm, similar to the length of the axis over which the load moves. In CASE 6, the length of the contour was 33mm also similar to the length over which the load moves, indicating the importance for future testing to capture the scale of arc movement. Like previous cases the 300ºC contour is severely elongated again; there is little change in the width of the contour from the plate centre to the plate edge.

One feature of the CASE 6 and 7 results is the slight non-symmetrical distribution of temperature. This may result from the speed of the moving arc (every 2.5×10^{-6} seconds). The speed of load movement is unknown from the preceding experimental work. CASE 8 models a faster moving arc (by a factor of 2.5). The predicted area above 500°C increased by 4% with the length of the contour approximately the same (increasing by 1 mm). Significantly the increased arc speed results in an increase in the predicted area above 800°C – the temperature at which complete resin decomposition is modelled to occur. The width of the 300ºC contour also reduces from the plate centre to the plate edge similar to experimental moderate damage.

4.5 Combined arc expansion and arc movement results

One final simulation considers combined arc expansion and arc movement (CASE 9). In this simulation a fixed radius filament moving as described in CASE 7 is applied along with an elliptical expanding arc (as defined in CASE 4). 50% of the current load is applied through the moving radius filament and 50% of the current load is applied through the expanding arc which applies a uniform current load. As before the same total current load (i.e. action interval) and the same rate of current load is applied.

Figure 9 presents the temperature contours for the simulation results and Table 5 presents the predicted area above 500 °C. Examining these final results the predicted surface area over 500°C is towards the upper bound of the previous simulations with clear portions of the area above 500°C oriented along the 0° axis (the direction of modelled arc movement) and oriented along the +45° axis (the surface fibre direction). From the cross-sectional view of the specimen, Figure 10, the 500°C zone reaches the fifth ply and is wedge shaped similar to experimental severe damage. Examining the development of temperature with time

through the thickness of the specimen, Figure 11, the temperatures above 500°C occur on the top surface of the specimen before propagating through the specimen thickness. This suggests the opportunity for gas from material decomposition to be trapped and cause further damage will be limited.

4.6 Results summary

All predicted thermal damage areas are smaller than the total measured damage in the specimens and this is sensible if we expect the witnessed mechanical damage behaviour to come from mechanical effects such as pressure loading and thermal expansion. Given the finding of recent preceding work that pressure is not significant [25-26] this indicates the need to model the mechanical behaviour of thermal expansion.

For the first time experimentally observed arc behaviours have been simulated. The predictions of temperature profiles which will result in material damage have been demonstrated to be sensitive to the modelling of arc expansion and movement. Measurements of the arc behaviour in further experimental tests are required to improve the representation of electrical loading.

5.0 Conclusions

Previous simulation studies of lightning strike direct effects on composite materials have overlooked or idealised the observed arc attachment behaviour witnessed in experimental tests. This is significant as these preceding studies have also demonstrated resistive heating is a major contributor to composite material damage. Herein a series of simulation studies have

modelled arc attachment behaviour, in the form of arc expansion and arc movement, using well established modelling approaches for composite damage prediction and coupled these with new methods to represent the described experimental arc attachment behaviour from the literature. The simulation studies have quantified the significance of arc attachment behaviour, demonstrating how realistic representation of arc expansion and arc movement will change the prediction of thermal loading. A major conclusion from this study is the need to experimentally capture, in a quantifiable fashion, arc attachment behaviour during artificial lightning strike tests. Without such data it is not possible to represent the current loading to a specimen and therefore take full advantage of the available computational simulation tools to accurately predict specimen thermal loading and thus predict damage.

Acknowledgment

Financial support from the Department for Employment and Learning, Northern Ireland for the Ph.D. research of P. Foster is gratefully acknowledged.

6.0 References

[1] M. Gagne, D. Therriault. Lightning Strike Protection of Composites. Progress in Aerospace Sciences, Vol. 64, pp. 1–16, 2014

[2] G. F. Abdelal and A. Murphy, "A multiphysics simulation approach for efficient modeling of lightning strike tests on aircraft structures," IEEE Trans. Plasma Sci., Vol. 45, no. 4, pp. 725–735, 2017.

[3] A. Katunin, K. Krukiewicz, R. Turczyn, P. Sul, K. Dragan. Lightning strike resistance of an electrically conductive CFRP with a CSA-doped PANI/epoxy matrix. Composite Structures, Vol. 181, 2017, pp. 203-213

[4] A. Katunin, K. Krukiewicz, R. Turczyn, P. Sul, A. Łasica, M. Bilewicz. Synthesis and characterization of the electrically conductive polymeric composite for lightning strike protection of aircraft structures. Composite Structures, Vol. 159, 2017, pp. 773-783

[5] F.S. Wang, Y.Y. Ji, X.S. Yu, H. Chen, Z.F. Yue. Ablation damage assessment of aircraft carbon fiber/epoxy composite and its protection structures suffered from lightning strike, Composite Structures, Vol. 145, 2016, pp. 226-241

[6] K. Fu, L. Ye, L. Chang, C. Yang, Z. Zhang. Modelling of lightning strike damage to CFRP composites with an advanced protection system. Part I: Thermal–electrical transition, Composite Structures, Vol. 165, 2017, pp. 83-90

[7] Y. Kostogorova-Beller, T. Lu. Numerical Modelling of Experimentally Obtained Lightning Arc Root Damage in Metal Sheets. International Journal of Engineering Practical Research, Vol. 2, pp. 139–146, 2013

[8] P. Lalande, A. Bondiou-Clergerie and P. Laroche – Analysis of Available In-Flight Measurements of Lightning Strikes to Aircraft. ICOLSE Toulouse, 1999

[9] J. Moreau, J. Alliot, and V. Mazur. Aircraft Lightning Initiation and Interception from In Situ Electric Measurements and Fast Video Observations. Journal of Geophysical Research, Vol. 97, Issue D14, pp. 15903–15912, 1992

[10] Aerospace Recommended Practice ARP 5412. Aircraft Lightning Environment and Related Test Waveforms, 1999. SAE.

[11] Aerospace Recommended Practice ARP 5414. Aircraft Lightning Zoning, 1999. SAE.

[12] Q. Dong, Y. Guo, J. Chen, X. Yao, X. Yi, L. Ping, Y. Jia. Influencing factor analysis based on electrical–thermal-pyrolytic simulation of carbon fiber composites lightning damage. Composite Structures, Vol. 140, 2016, pp. 1-10

[13] Y. Li, T. Xue, R. Li, X. Huang, L. Zeng. Influence of a fiberglass layer on the lightning strike damage response of CFRP laminates in the dry and hygrothermal environments. Composite Structures, Vol. 187, 2018, pp. 179-189

[14] A. Todoroki, K. Ohara, Y. Mizutani, Y. Suzuki, R. Matsuzaki. Lightning strike damage detection at a fastener using self-sensing TDR of composite plate, Composite Structures, Vol. 132, 2015, pp. 1105-1112

[15] S. Haigh. Impulse Effects During Simulated Lightning Attachments to Lightweight Composite Panels. Presented at Int. Aerospace Ground Conf. on Lightning and Static Electricity, Paris, France. 2007

[16] P. Feraboli and M. Miller. Damage resistance and tolerance of carbon/epoxy composite coupons subjected to simulated lightning strike. (98195-2400), Presented at AIAA/ASME/ASCE/AHS/ASC Structures, Structural Dynamics and Materials Conference, Palm Springs, California. 2009

[17] Y. Hirano, S. Katsumata, Y. Iwahori, and A. Todoroki. Artificial Lightning Testing on Graphite/Epoxy Composite Laminate. Composites Part A: Applied Science and Manufacturing, Vol. 41, Issue 10, pp. 1461-1470, 2010

[18] P. Feraboli and H. Kawakami. Damage of Carbon/Epoxy Composite Plates Subjected to Mechanical Impact and Simulated Lightning. Journal of Aircraft, Vol. 47, No. 3, 2010

[19] J. Gou and Y. Tang and F. Liang and Z. Zhao. Carbon Nanofiber Paper for Lightning Strike Protection of Composite Materials. Composites: Part B, Vol. 41 (1359-8368), pp 192-198, 2010

[20] H. Kawakami. Lightning strike induced damage mechanisms of carbon fiber composites. PhD Thesis, University of Washington, 2011.

[21] H. Kawakami and P. Feraboli. Lightning Strike Damage Resistance and Tolerance of Scarf-Repaired Mesh-Protected Carbon Fiber Composites. Composites: Part A, Vol. 42, pp. 1247–1262, 2011.

[22] L. Chemartin, P. Lalande, B. Peyrou, A. Cahzottes, and P. Elias. Direct Affects of Lightning on Aircraft Structure: Analysis of the Thermal, Electrical and Mechanical Constraints. Journal of Aerospace Lab, Vol. 5, 2012

[23] N. Hosokawa, T. Ooto, S. Kubo, M. Anzai, A. Yoshiya, and A. Nakagoshi. Lightning strike protection for composite laminates by pitch-based carbon fibre skin. Presented at The 19th International Conference on Composite Materials, Montreal, Canada. 2013

[24] S. Yamashita, I. Ohsawa, A. Morita, and J. Takahashi. Fracture behaviour of carbon fibre reinforced polypropylene under artificial lightning strike. Presented at The 19th International Conference on Composite Materials, Montreal, Canada, 2013

[25] R. Munoz, S. Delgado, C. Gonzalez, B. Lopez-Romano, D. Wang, and J. Llorca. Modelling lightning impact thermo-mechanical damage on composite materials. Applied Composite Materials, Vol. 21, Issue 1, pp 149–164. 2014

[26] P. Foster, G. Abdelal, A. Murphy. Quantifying the Influence of Lightning Strike Pressure Loading on Composite Specimen Damage, Under journal review with the International Journal for the Science and Application of Composite Materials.

[27] Y. Shi, T. Swait, C. Soutis, Modelling damage evolution in composite laminates subjected to low velocity impact, Composite Structures, Vol. 94, Issue 9, pp. 2902-2913, 2012

[28] Vaibhav A. Phadnis, Puneet Kumar, Arun Shukla, Anish Roy, Vadim V. Silberschmidt, Optimising curvature of carbon fibre-reinforced polymer composite panel for improved blast resistance: Finite-element analysis, Materials & Design, Vol. 57, pp. 719-727, 2014

[29] T. Ogasawara, Y. Hirano, A. Yoshimura. Coupled Thermal-Electrical Analysis for Carbon Fiber/Epoxy Composites Exposed To Simulated Lightning Strike. Composites Part A: Applied Science and Manufacturing, Vol. 41, Issue 8, pp. 973-981, 2010

[30] G. Abdelal, A. Murphy, Nonlinear numerical modelling of lightning strike effect on composite panels with temperature dependent material properties, Composite Structures, Vol. 109, pp. 268-278, 2014

[31] F. Wang, N. Ding, Z. Liu, Y. Ji, and Z. Yue. Ablation damage characteristic and residual strength prediction of carbon fibre/epoxy composite suffered from lightning strike. Composite Structures, Vol. 117, pp. 222-233, 2014

[32] Q. Dong, Y. Guo, X. Sun, and Y. Jia. Coupled electrical-thermal-pyrolytic analysis of carbon fiber/epoxy composites subjected to lightning strike. Polymer, Vol. 56, pp. 385-394, 2015

[33] Z. Liu, Z. Yue, F. Wang, Y. Ji. Combining analysis of coupled electrical-thermal and blow-off impulse effects on composite laminate induced by lightning strike. Applied Composite Materials. Vol. 22, Issue 2, pp 189–207, 2015

[34] T. Kirchdoerfer, A. Liebscher, M. Ortiz, CTH Shock Physics Simulation of Non-linear Material Effects within an Aerospace CFRP Fastener Assembly due to Direct Lightning Attachment, Composite Structures, 2018, , ISSN 0263-8223, https://doi.org/10.1016/j.compstruct.2017.11.061

[35] Fulmen Report: Investigation of the parameters affecting mechanical forces in aluminium and cfc plates subject to simulated lightning strikes. Transport Research and Technological Development Program. 1997

[36] E. Rupke. Lightning Direct Effects Handbook. Advanced General Aviation Transport Experiments. 2002

[37] Y. Wang, O. Zhupanska. Lightning strike thermal damage model for glass fiber reinforced polymer matrix composites and its application to wind turbine blades. Composite Strcutures. Vol. 132, pp 1182–1191, 2015

[38] Anon. ABAQUS Theory Manual. Dassault Systèmes. 2012

[39] Y. Li, T. Xue, R. Li, X. Huang, L. Zeng. Influence of a fiberglass layer on the lightning strike damage response of CFRP laminates in the dry and hygrothermal environments. Composite Strcutures. Vol. 187, pp 179–189, 2018

[40] J. Fanucci. Thermal response of radiantly heated Kevlar and graphite/epoxy composites. Journal of Composite Materials. Vol. 21, pp 129–139, 1987

[41] Y. Wang, O.I. Zhupanska. Modeling of thermal response and ablation in laminated glass fiber reinforced polymer matrix composites due to lightning strike. Applied Mathematical Modelling, Vol. 53, pp. 118-131, 2018

Tables

Table 1 – Temperature dependent material properties.

Temperature dependent material properties				
		Thermal Conductivity		
Temperature (°C)	Specific Heat (J/kg °C)	Fibre (W/mm.K)	Transverse (W/mm.K)	Through-Thickness (W/mm.K)
25	1065	0.008	0.00067	0.00067
500	2100	0.004390	0.000342	0.000342
800	2100	0.002608	0.00018	0.00018
1000	2171	0.001736	0.0001	0.0001
3316	2500	0.001736	0.0001	0.0001
3334*	5875	0.001736	0.0001	0.0001
3335*	5875	0.0005	0.0005	0.0005
7000*	5875	0.001015	0.001015	0.001015
Temperature dependent material properties				
		Electrical Conductivity		
Temperature (°C)	Density (kg/mm^3)	Fibre (1/ Ω.mm)	Transverse (1/ Ω.mm)	Through-Thickness (1/ Ω.mm)
25	1.52×10^{-6}	35.97	0.001145	1.79×10^{-6}
500	1.52×10^{-6}	35.97	0.001145	1.79×10^{-6}
800	1.10×10^{-6}	35.97	0.001145	1.79×10^{-6}
3316	1.10×10^{-6}	35.97	0.001145	1.79×10^{-6}
3334*	1.11×10^{-9}	35.97	2	1×10^{6}
3335*	1.11×10^{-9}	0.2	0.2	1×10^{6}
7000*	1.11×10^{-9}	1.5	1.5	1×10^{6}
* - *Gas*				

Table 2 – Experimental damage areas compared with simulated temperature areas above 500°C (CASE 1, 2 and 3).

Experimental Specimen	Moderate damage area			Severe damage area		
	Area (mm^2)	Max. dim. (mm)	Shape/ Orientation	Area (mm^2)	Max. dim. (mm)	Shape/ Orientation
B-4	2,356	76 x 62	diamond/ +45 °	975	44 x 24	rectangular/ 0 °
C2-1	2,010	67 x 60	diamond/ +45 °	950	42 x 32	square/ +45 °

Simulation CASE	Peak temperature above 500 °C contour		Peak temperature above 300 °C contour
	Area (mm^2)	Length (mm)	Shape/ Orientation
1	430	69	Narrow, contour width slightly decreases from centre to plate edge / +45 °
2	450	30	Contour width slightly decreases from centre to plate edge / +45 °
3	660	72	Elongation both at centre and extreme width / +45 °

Table 3 – Experimental damage areas compared with simulated temperature areas above 500°C (CASE 4 and 5).

Experimental Specimen	Moderate damage area			Severe damage area		
	Area (mm^2)	Max. dim. (mm)	Shape/ Orientation	Area (mm^2)	Max. dim. (mm)	Shape/ Orientation
B-4	2,356	76 x 62	diamond/ +45 °	975	44 x 24	rectangular/ 0 °
C2-1	2,010	67 x 60	diamond/ +45 °	950	42 x 32	square/ +45 °

Simulation CASE	Peak temperature above 500 °C contour		Peak temperature above 300 °C contour
	Area (mm^2)	Length (mm)	Shape/ Orientation
4	420	50	centre to plate edge / +45 °
5	350	31	centre / +45 °

Table 4 – Experimental damage areas compared with simulated temperature areas above 500°C (CASE 6, 7 and 8).

Experimental Specimen	Moderate damage area			Severe damage area		
	Area (mm^2)	Max. dim. (mm)	Shape/ Orientation	Area (mm^2)	Max. dim. (mm)	Shape/ Orientation
B-4	2,356	76 x 62	diamond/ +45 °	975	44 x 24	rectangular/ 0 °
C2-1	2,010	67 x 60	diamond/ +45 °	950	42 x 32	square/ +45 °

Simulation CASE	Peak temperature above 500 °C contour		Peak temperature above 300 °C contour
	Area (mm^2)	Length (mm)	Shape/ Orientation
6	820	33	Decrease in contour width from centre to plate edge / +45 °
7	910	41	Decrease in contour width from centre to plate edge / +45 °
8	950	42	Decrease in contour width from centre to plate edge / +45 °

Table 5 – Experimental damage areas compared with simulated temperature areas above 500°C (CASE 9).

Experimental Specimen	Moderate damage area			Severe damage area		
	Area (mm^2)	Max. dim. (mm)	Shape/ Orientation	Area (mm^2)	Max. dim. (mm)	Shape/ Orientation
B-4	2,356	76 x 62	diamond/ -45 °	975	44 x 24	rectangular/ 0 °
C2-1	2,010	67 x 60	diamond/ -45 °	950	42 x 32	square/ +45 °

Simulation CASE	Peak temperature above 500 °C contour		Peak temperature above 300 °C contour
	Area (mm^2)	Length (mm)	Shape/ Orientation
9	945	37.5	Decrease in contour width from centre to plate edge / +45 °

Figures:

Specimen B-4	Specimen C2-1
<u>Severe damage</u> - Characterise by an absence and/or broken fibres, with the majority of surface resin absent.	
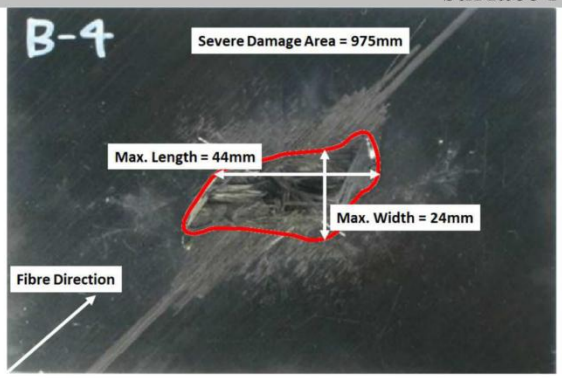	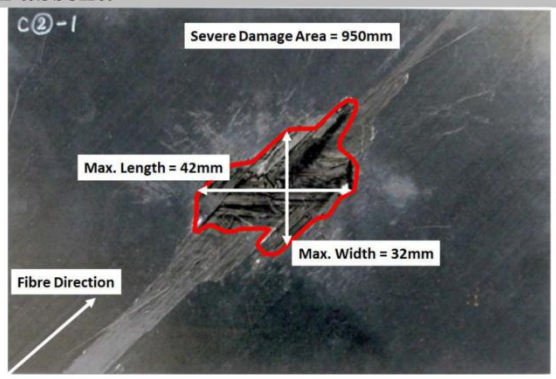
Maximum damage depth ≈ 0.735 mm	Maximum damage depth ≈ 0.735 mm
<u>Moderate damage</u> - Characterise by an absence of some surface resin, may also include limited fibre burst out and/or fracture	
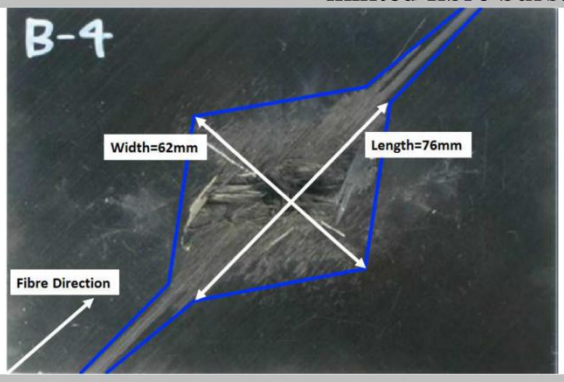	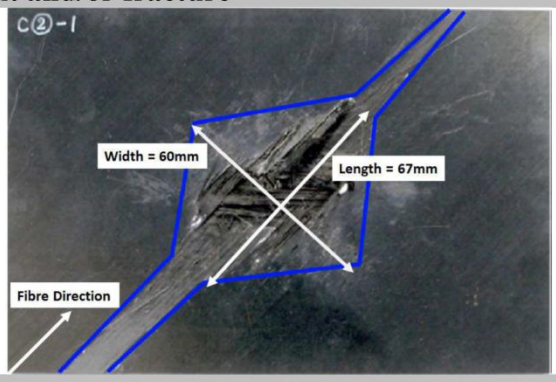
<u>Subsurface damage</u> - Including intralaminar and interlaminar matrix cracking	
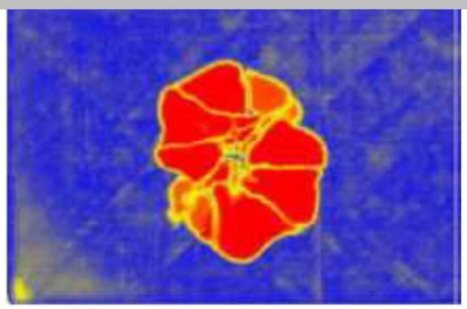	Not available
Maximum damage depth ≈ 1.1 mm	

Figure 1 – Damage areas identified from experiment with a peak current of 40kA, rise time from 10% to 90% of maximum current is 4μs and time through to 50% of maximum current is 20μs.

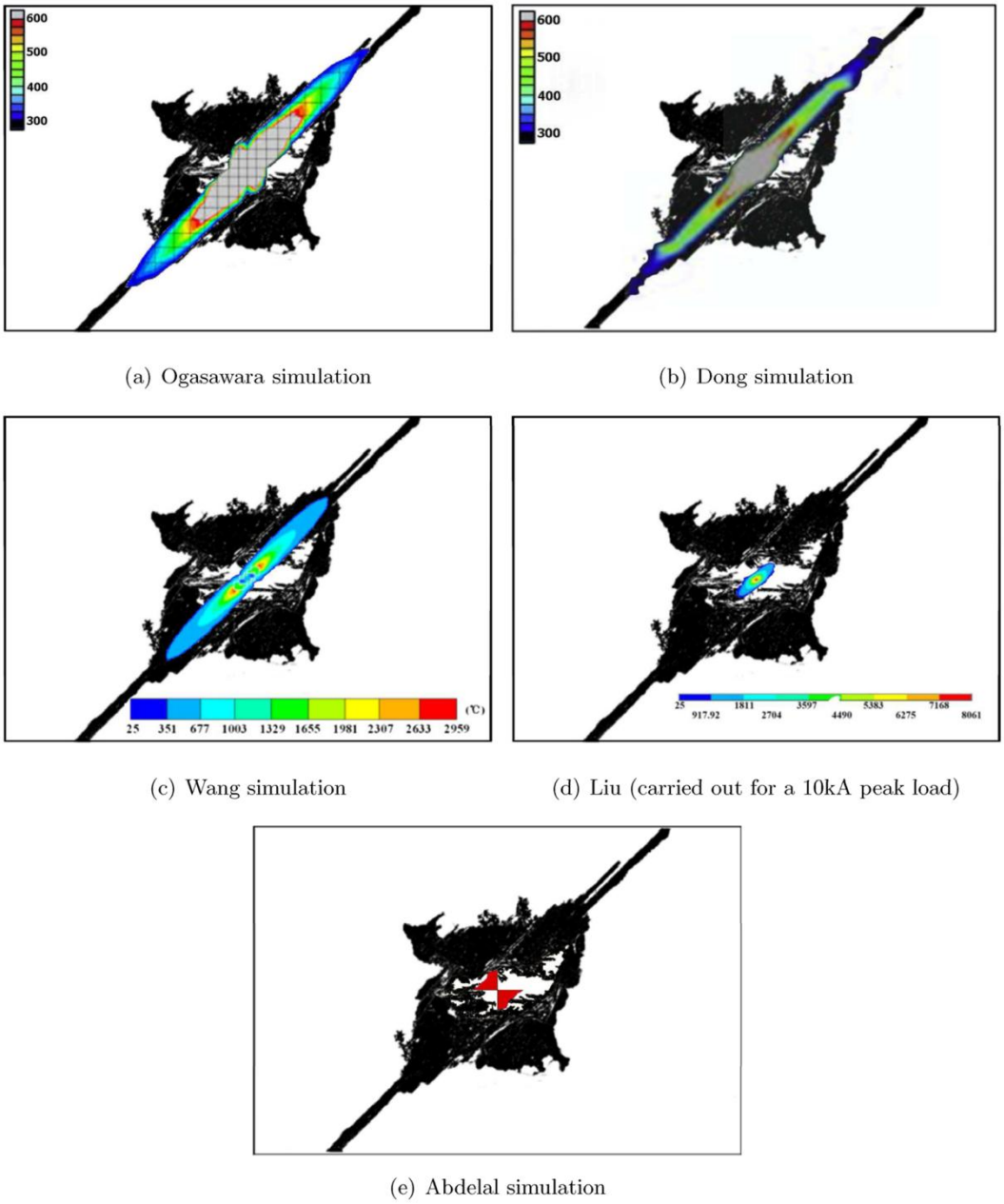

(a) Ogasawara simulation

(b) Dong simulation

(c) Wang simulation

(d) Liu (carried out for a 10kA peak load)

(e) Abdelal simulation

Figure 2 – Moderate damage area captured by image binarisation overlaid with temperature fields from simulations by previous authors.

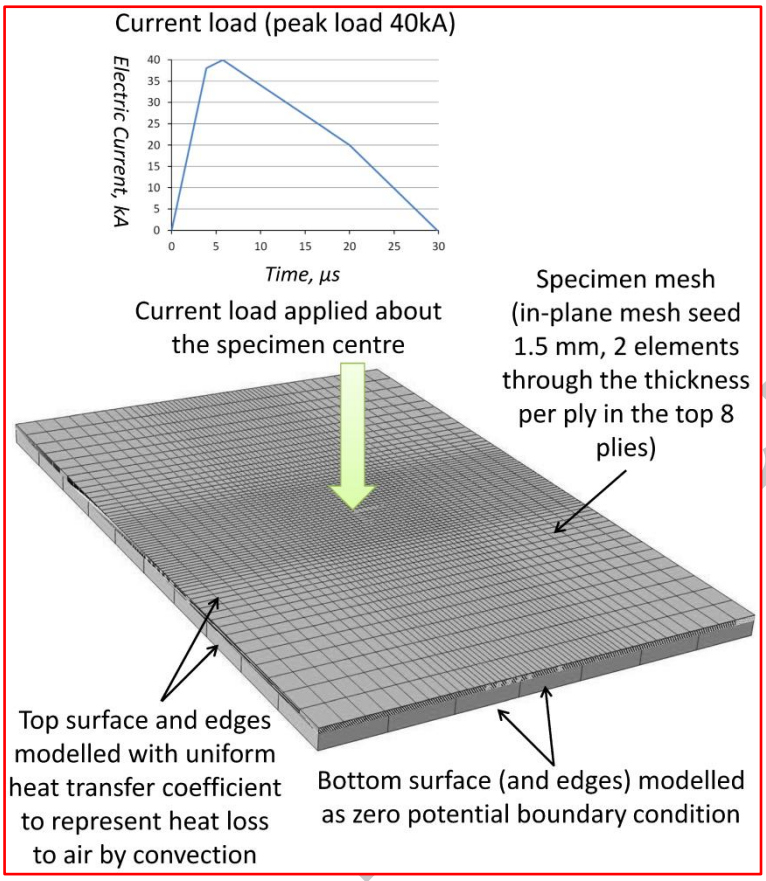

Figure 3 – Specimen mesh plus overview of analysis loading and boundary conditions.

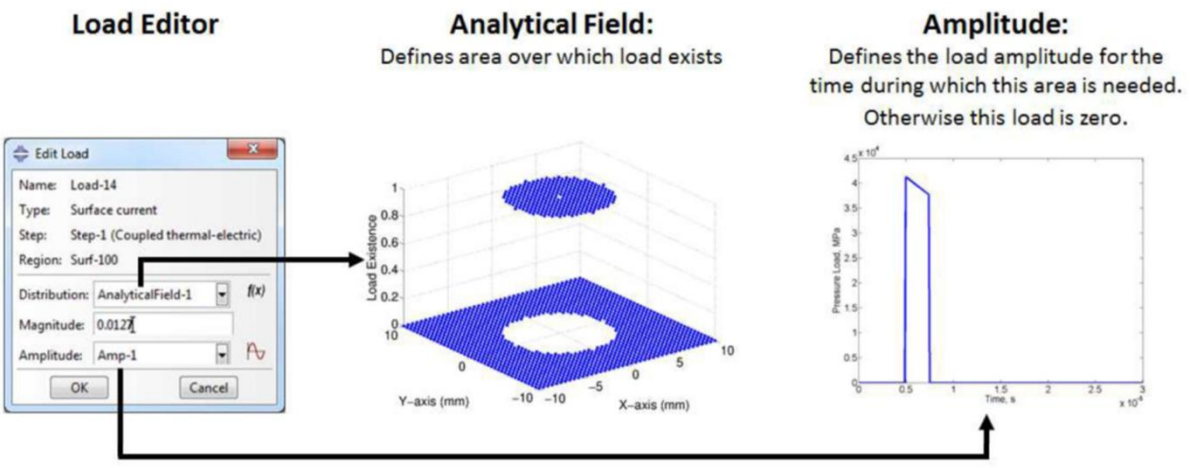

a)

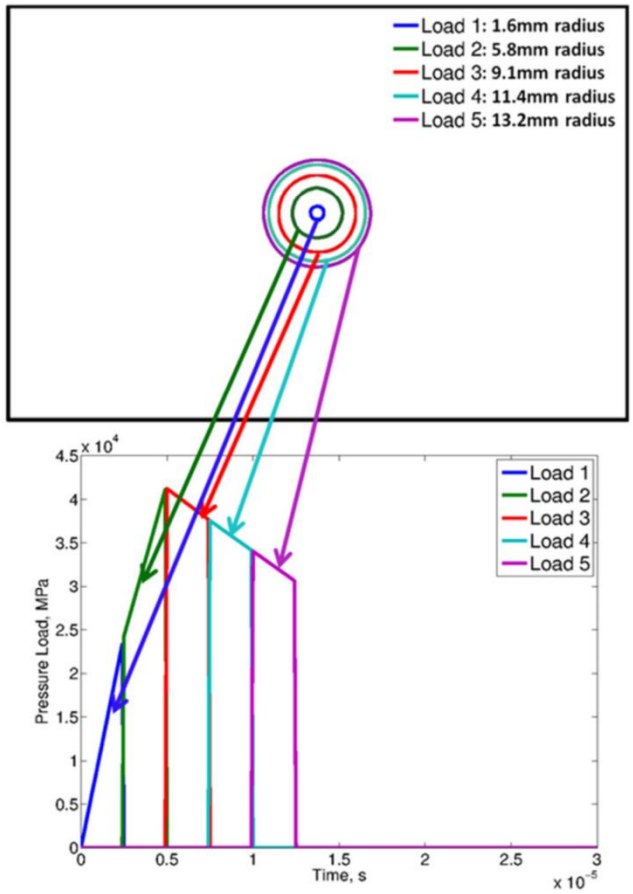

b)

Figure 4 – The implementation of the expanding arc radius: a) load editor through which the electrical surface current load is applied, b) The first five radii for the first five loads used to represent the expanding arc channel.

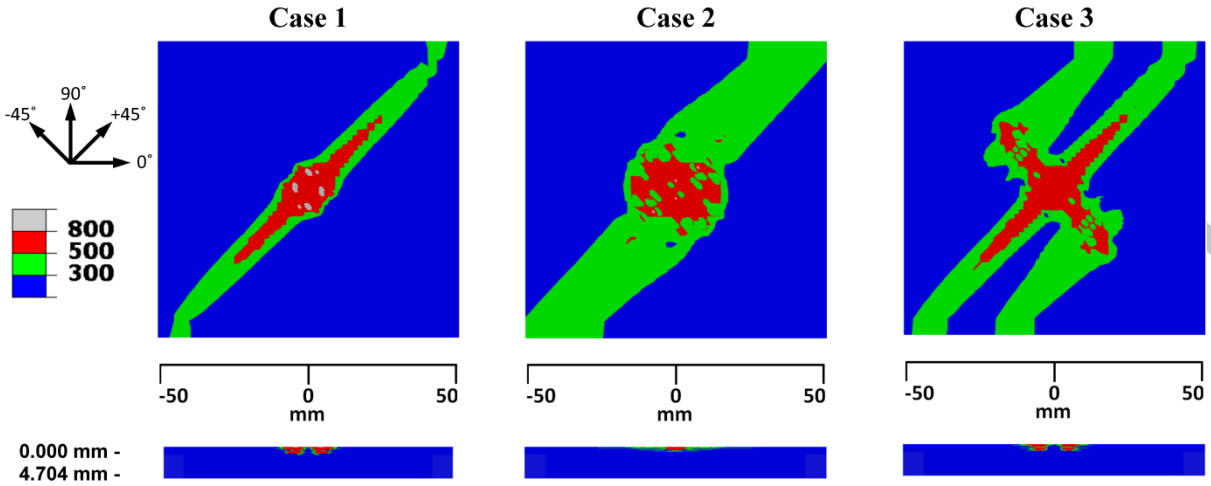

Figure 5 – Temperature contours for the simulation cases CASE 1, 2 and 3 (shown is the centre 100 x 100 mm of the specimen).

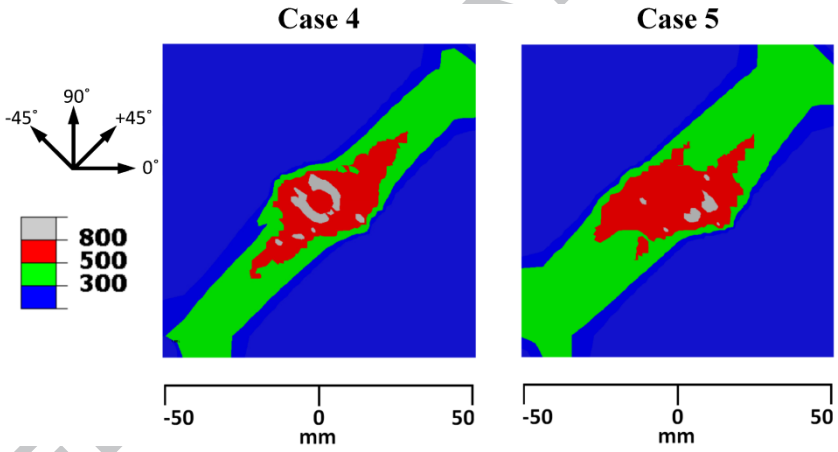

Figure 6 – Temperature contours for the simulation cases CASE 4 and 5 (shown is the centre 100 x 100 mm of the specimen).

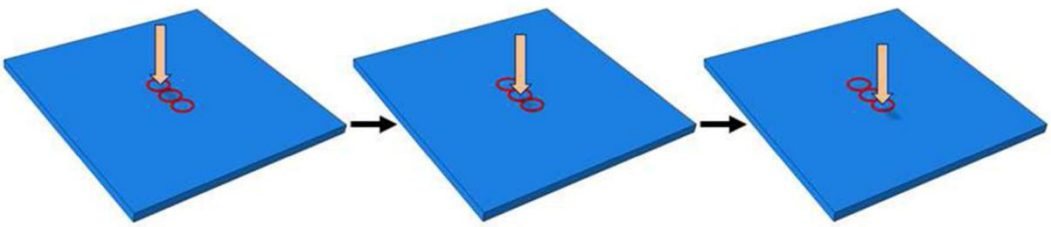

Figure 7 – Illustration of method to apply arc movement.

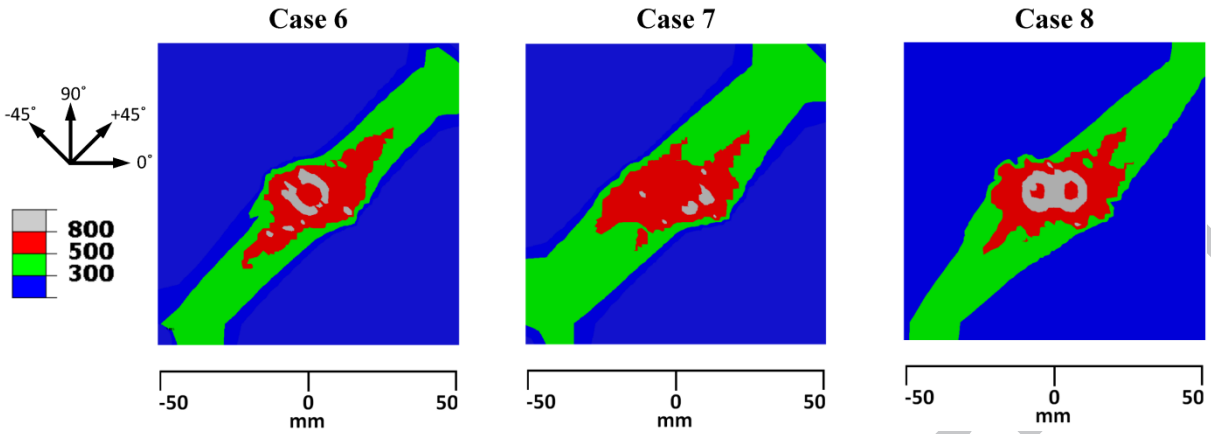

Figure 8 – Temperature contours for the simulation cases CASE 6, 7 and 8 (shown is the centre 100 x 100 mm of the specimen).

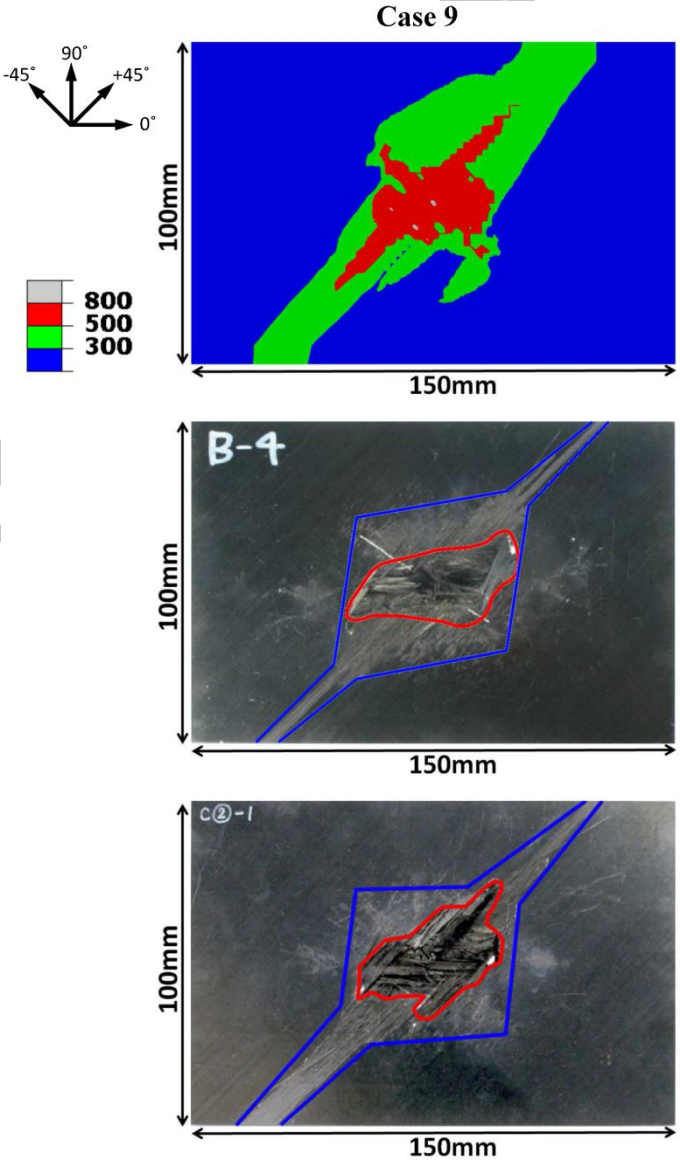

Figure 9 – Temperature contours for the simulation CASE 9, along with equivalent experimental damage images.

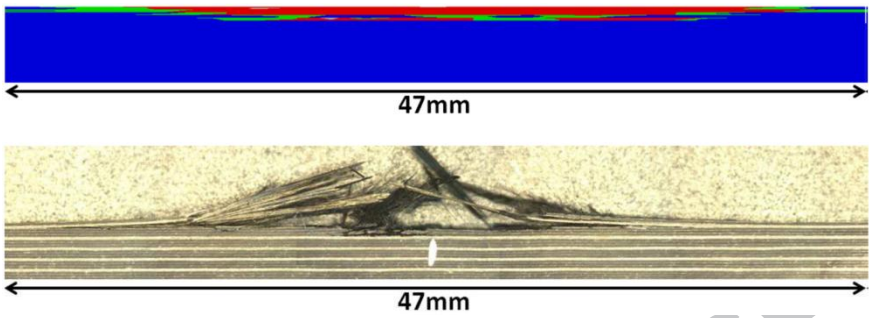

Figure 10 – Temperature contours for the simulation cases CASE 9 (shown is a cross-sectional view at the centre 47 mm of the specimen), along with an equivalent experimental damage image.

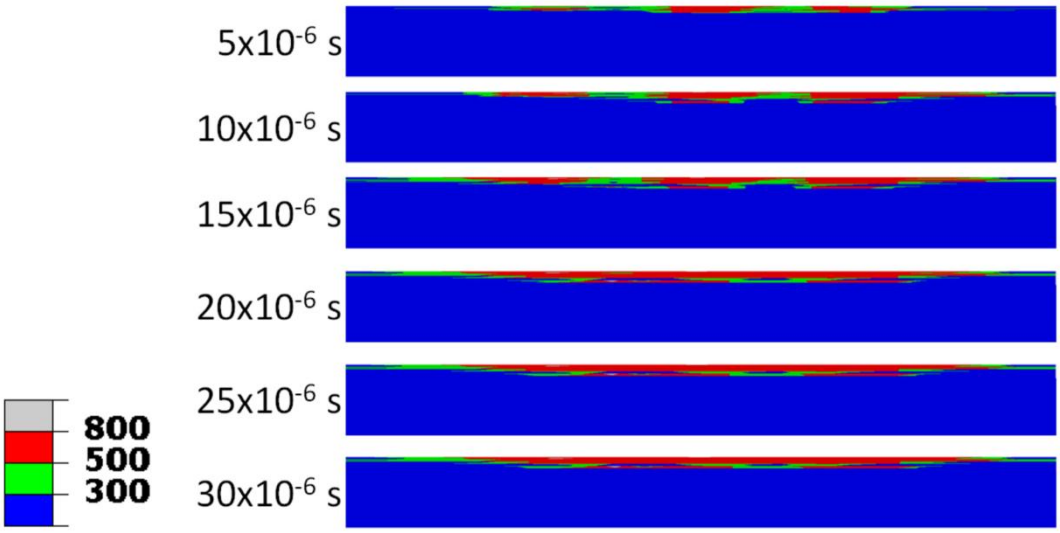

Figure 11 – Development of 500°C and 300°C contours from a cross-section through the centre of the plate.